1
2
Predicting efficiency of writing short sequences into the genome using prime editing

3
4 Jonas Koeppel[1,†] Elin Madli Peets[1,†], Juliane Weller[1,†], Ananth Pallaseni[1], Fabio Liberante[1], Leopold
5 Parts[1,2,*]
6
7 [1] Wellcome Sanger Institute, Wellcome Genome Campus, Hinxton, UK

8 [2] Department of Computer Science, University of Tartu, Tartu, Estonia

9 [†] These authors contributed equally to this work

10 * Corresponding author. Tel: +44 1223 834 244; E-mail: leopold.parts@sanger.ac.uk
11

12

SUMMARY

14 Short sequences can be precisely written into a selected genomic target using prime editing.
15 This ability facilitates protein tagging, correction of pathogenic deletions, and many other
16 exciting applications. However, it remains unclear what types of sequences prime editors can
17 easily insert, and how to choose optimal reagents for a desired outcome. To characterize
18 features that influence insertion efficiency, we designed a library of 2,666 sequences up to 69
19 nt in length and measured the frequency of their insertion into four genomic sites in three
20 human cell lines, using different prime editor systems. We discover that insertion sequence
21 length, nucleotide composition and secondary structure all affect insertion rates, and that
22 mismatch repair proficiency is a strong determinant for the shortest insertions. Combining the
23 sequence and repair features into a machine learning model, we can predict insertion
24 frequency for new sequences with R = 0.69. The tools we provide allow users to choose
25 optimal constructs for DNA insertion using prime editing.

INTRODUCTION

Efficient insertion of short DNA sequences into genomes could change the course of biotechnology and medicine. Small insertions can encode protein tags for purification and visualization, or allow manipulation of protein localization, half-life, and interaction profiles to control their function. Integrating sequences for transcription factor binding sites and splicing modulators provides control over gene expression, while introducing structural elements or recombinase sites can change DNA conformation and provide a substrate for large-scale engineering[1,2]. For therapeutic opportunities, over 16,000 small deletion variants have been causally linked to disease[3,4], and could in principle be restored by inserting the missing sequence[5,6]. A prominent example is cystic fibrosis, where 70% of cases are caused by a 3 nt deletion[7,8]. An ideal tool to enable these applications would integrate the edits efficiently, accurately, and safely, avoiding unintended outcomes or double strand break stress that has hampered Cas9-based therapies[9-11].

Prime editors can insert short DNA sequences without generating double-strand breaks or needing an external template. They consist of a nicking version of Cas9 fused to a reverse transcriptase domain, which is complexed with a prime editing guide RNA (pegRNA)[12]. The pegRNA comprises a primer binding site homologous to the sequence in the target, and a reverse transcriptase template that includes the intended edit, all in the 3' extension of a standard CRISPR/Cas9 guide RNA. At the target site, Cas9 nicks one strand of the genomic DNA, which then anneals to the primer binding site on the pegRNA, and is extended by the Cas9-fused reverse transcriptase using the pegRNA-encoded template sequence. Next, DNA repair mechanisms resolve the conflicting sequences on the two DNA strands, ultimately writing the intended edit into the genome. When CRISPR/Cas9 was compared to molecular scissors capable of disrupting target genes, and base editors were called molecular pencils for their ability to substitute single nucleotides, prime editors were described as molecular word processors able to perform search and replace operations directly on the genome[13].

The prime editing system is complex, and the determinants of its efficiency are not fully understood. Several partly independent steps, including three DNA binding events and a successful mismatch repair are needed to produce an edit, each potentially introducing biases. In the largest study so far to understand these biases, Kim et al. comprehensively tested the consequences of varying the reverse transcription templates and primer binding site lengths using a library of 55,000 pegRNAs. Editing rate increased with Cas9 gRNA activity, as well as

60 GC content and melting temperature of the primer binding site. Primer binding sites of 13 nt

61 and reverse transcriptase templates of 12 nt generally worked well[14].

62

63 The majority of libraries used by Kim *et al.* contained the same single nucleotide substitution

64 5 nt upstream of the nick site. Similarly, nearly all current characterization of prime editing

65 efficacy has predominantly focused on single nucleotide substitutions[12,15-18]. Of the many

66 possible useful sequences in molecular biology, only a handful have been introduced with

67 prime editing and the longest successfully reported insertion was 44 nt in length[12]. Therefore,

68 in contrast to relatively deep understanding of Cas9 mutagenesis[10,19-21] and base editing

69 outcomes[22-24] very little is known about how the inserted sequence affects efficiency, and the

70 length range of insertions feasible by prime editing has not been defined.

71

72 Here, we systematically measure the insertion efficiency of over 2,600 sequences and identify

73 the features responsible. We find that insertion sequence length, nucleotide composition,

74 secondary structure, and repair pathway activity together explain most of the variation in

75 insertion rate. We then use these insights to train a sequence-based prediction model

76 informed by mismatch repair efficiency that predicts editing outcomes for novel sequences

77 with high accuracy, and allows selection of optimal reagents for new insertions.

78 **RESULTS**

79 We sought to systematically characterize how the length and composition of inserted

80 sequence, as well as cell line, target site, and the version of the prime editor system affect

81 insertion rates. To do so, we designed 2,666 pegRNAs encoding insertions immediately

82 upstream of the nick site. These comprise 270 sequences useful for molecular biology

83 (including e.g. His-6 tag, recombinase sites, and mNeonGreen11[25]), 1,957 eukaryotic linear

84 motifs[26,27], and 439 sequences with variable secondary structure (Figure 1a). The insertion

85 lengths ranged from 1 to 69 nt, with varied GC content (Figure 1b). We used lentiviruses to

86 deliver the library against four target sites (three previously tested: HEK3, EMX1, FANCF[12]

87 and the safe-harbor CLYBL locus[28]) in two cell lines (HEK293T and HAP1), followed by

88 transient transfection of the prime editor plasmid, five days of selection, and sequencing of

89 two amplicons from the cell pool, one of the targeted locus and one of the pegRNA locus

90 (Figure 1c). We calculated insertion efficiencies as the fraction of reads in the target site

91 amplicon with a given insertion divided by the fraction of reads for the pegRNA encoding it in

92 the pegRNA amplicon, and analyse them as the main statistic in the rest of the study.
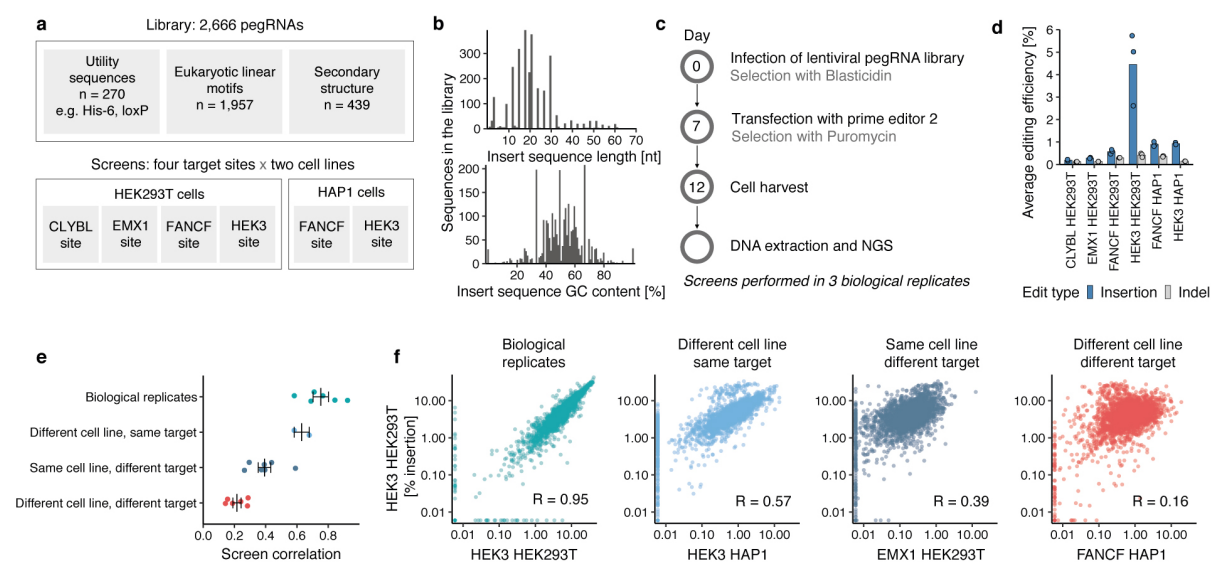
Figure 1. High-throughput measurement of prime insertion efficiencies. a. Screen setup. **b.** Library composition. Number of sequences in the library (y-axis) with different insert sequence lengths (x-axis, top panel) and %GC content (x-axis, bottom panel). **c.** Experimental design **d.** Editing frequencies. Average mutation frequency (y-axis) for different screens (x-axis) stratified by mutation type (blue: insertions; grey: indels). Markers represent one replicate and bars the average across *n*=3 biological replicates. **e.** Replicate concordance. Pearson's R between insertion rates in two screens (x-axis) for different comparisons (y-axis, colors). Markers: correlation value of one pair of screens (for replicate correlations, mean of pairwise comparison across *n*=3 biological replicates); line and whiskers: mean and standard error of mean. **f.** Representative examples of categories from (e). Percent insertion in the HEK3 locus in HEK293T cells (y-axis) compared to values (x-axis) in other contexts (panels, colors) for insertion sequences (markers). Left panel: comparison of biological replicates; other panels: comparison of replicate averages. Label: Pearson's R of values in linear scale. Colors: as in (e).

Insertion efficiencies of pegRNAs varied widely. The top 1% of pegRNAs were inserted 210-2,040 times more efficiently than the bottom 1% across the various target site and cell line combinations (Supplementary Figure 1a), indicating substantial sequence-dependent variation. The insertion rates were highly consistent across biological replicates (average Pearson's R=0.76, range 0.64-0.95; Supplementary Figure 1b), but differed in magnitude across screens (average across pegRNAs 0.19% for CLYBL locus in HEK293T to 4.45% for HEK3 locus in HEK293T cells, Figure 1d). Small insertions and deletions around the target site were rare (0.12%-0.42%, Figure 1d), as were additional single-nucleotide mutations around the nicking site derived from the prime editing process (0.03% on average in reads with an inserted sequence vs 0.03% in reads without insertions, Supplementary Figure 1c). Overall, the intended insertions were the dominant mutations generated, and we do not consider the unintended edits further.

4

120   To understand the consistency of insertion efficiencies across contexts, we next compared

121   them between replicates, cell lines, and target sites. Insertion rates into the same target site

122   in different cell lines were more correlated (mean Pearson's R=0.63) than into different target

123   sites in the same line (mean Pearson's R=0.39), indicating a greater dependence on target

124   locus than cellular background. The correlation was weakest when both target site and cell

125   line were different (mean Pearson's R=0.22, Figure 1e-f), demonstrating both target

126   sequence-specific, and cell line-dependent biases on insertion.

127   **Insert size effects**

128   Given the repeatable sequence dependent variation in insertion rates that spans over three

129   orders of magnitude, we sought to understand the responsible features. We first asked how

130   insert sequence length affects insertion efficiency. For HEK293T cells, sequences of up to

131   4 nt (all four single nucleotides, all 16 dinucleotides, and 63 trinucleotides) were inserted on

132   average 2.1-4.6 times more efficiently than longer ones across the four targeted sites (Figure

133   2a). Insertion frequency did not decrease monotonically with increasing insert length, as

134   sequences between 15 and 21 nt were inserted 1.3-1.6 times more efficiently than 10-14 nt

135   ones (Figure 2a). These relative biases in efficiency were shared between all target sites,

136   despite a 20-fold range of their average insertion rates. Inserts longer than 45 nt were

137   incorporated less frequently, albeit at a screen average rate of 22-38% of sequences shorter

138   than 45 nt. The longest sequence that was inserted at > 1% frequency (1.4%, HEK3 site in

139   HEK293T cells) was 66 nt, demonstrating that reasonably efficient integration of moderately

140   long sequences is feasible with prime editing.

141

142   In contrast to HEK293T cells, insertion frequency of the short 1-4 nt sequences was 1.2 to

143   3.7-fold lower than that for longer ones in HAP1 cells (Figure 2b). This reduced the correlation

144   of insertion rates between the two cell lines at the same site compared to replicate correlation

145   (Pearson's R=0.68 for FANCF and 0.57 for HEK3, Figure 2b; median replicate correlation

146   R=0.75, Supplementary Figure 2a). However, stratifying the inserted sequences by length

147   recovers strong concordance, with correlations between rates in HAP1 and HEK293 cells at

148   the HEK3 locus increasing to 0.67, 0.78, and 0.80, respectively, for sequences of lengths 1-4

149   nt, 5-15 nt, and 16-70 nt. This correlation within length bins indicates consistent pegRNA

150   effects, while the discordance between bin averages across lines (but not targets in the same

151   line) hints that the cellular context does not influence inserts of different lengths in the same

152   way. One possible explanation is mismatch repair (MMR) proficiency, since HEK293T cells

153   are partly MMR deficient due to promoter methylation of MLH1[29], while HAP1 cells are not.

154   The MMR pathway recognizes and excises short mismatches of less than 13 nt and could

155   therefore remove short insertions in HAP1 cells before the nicked strand is re-ligated[17,30].

156
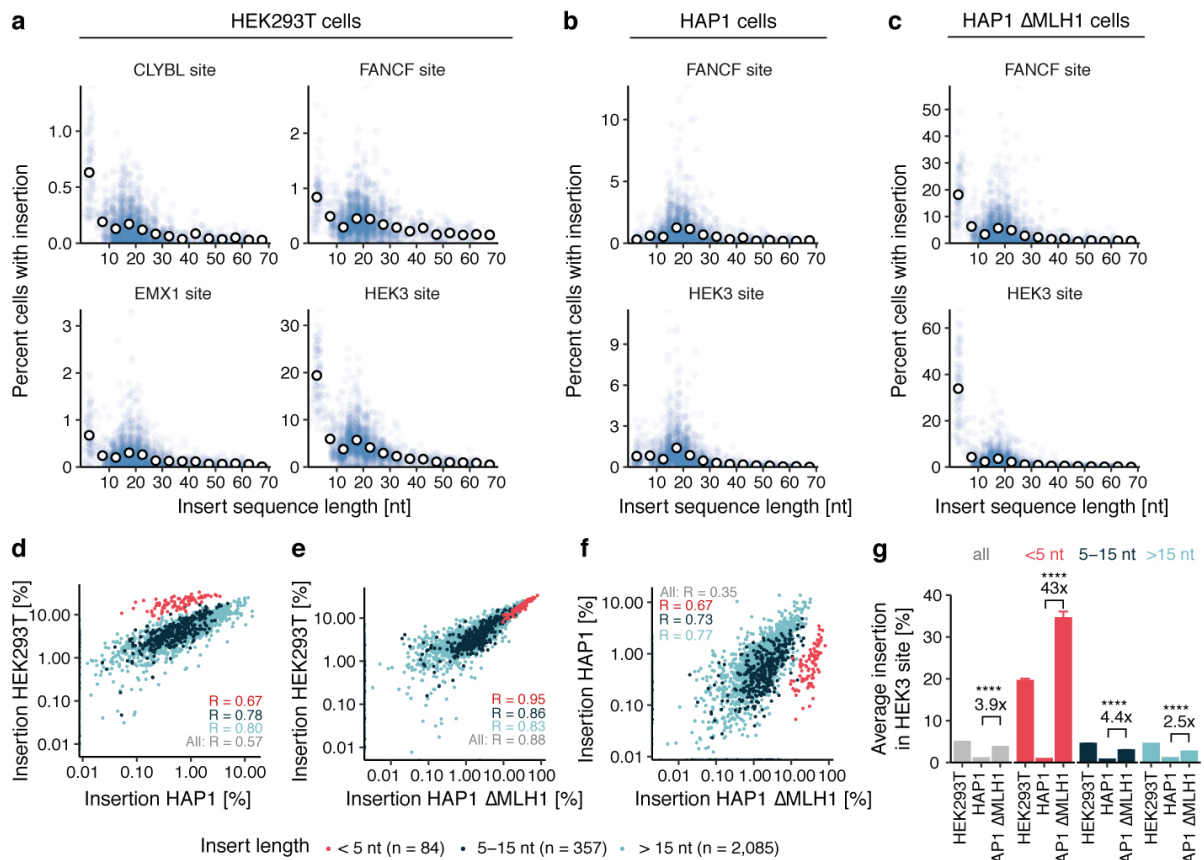
157
158   **Figure 2. Prime insertion efficiency depends on insert length. a.** Insertion rate in HEK293T cells.

159   Percent cells with insertion (y-axis) for different insert sizes (x-axis) of individual sequences (blue

160   markers) and their averages in 5nt length bins (white markers) at different target sites (panels). Data

161   represent the average of *n*=3 biological replicates. **b.** As a), but for HAP1 cells. **c.** As a), but for HAP1

162   ΔMLH1 cells. **d.** Insertion rate in HEK293T cells (y-axis) compared to rate in HAP1 cells (x-axis) at the

163   HEK3 target of individual sequences (markers). Red: short sequences (up to 4nt); blue: medium

164   sequences (5-15nt); teal: longer sequences (>15nt). Label: Pearson's R between rates. The data are

165   an average from *n*=3 biological replicates. **e-f).** As (d), but comparing insertion rates in HAP1 ΔMLH1

166   cells with HEK293T cells (e) and HAP1 wild type cells (f). **g.** MLH1 knockout increases insertion rates

167   disproportionately for short sequences. Average insertion rates at the HEK3 locus (y-axis) across

168   different cellular contexts (x-axis) for different length bins (colors). Comparison: ratio of average

169   insertion rate between HAP1 ΔMLH1 cells and HAP1 wild type cells; p-values (all < 1x10^{-33}) from two-

170   sided Student's t-test. Error bars: standard error of the mean. Colors as in (d)-(f).

171

172   To test the hypothesis that rates of inserting short sequences differ between cell lines due to

173   mismatch repair activity, we screened the HEK3 and FANCF-targeted libraries in HAP1 cells

174   that are knockout for MLH1 (HAP1 ΔMLH1, Supplementary Figure 2b,c). We found that

175   average insertion rates increased 3.9 to 5.1-fold in the mutant background compared to wild

176   type HAP1 cells. The rates 1-4 nt sequences were most affected, increasing by 43-66 fold to

177   19-34%, while the rates of 5-15 nt and >15 nt sequences increased 4.4-7.9 fold and 2.5-4.2

178   fold, respectively (Figure 2g, Supplementary Figure 2d,e). These remarkable increases in

179   insertion rates for short sequences are consistent with a model where MMR predominantly

180   recognizes short insertions, and thereby antagonizes prime editing. Indeed, for the HEK3

181   target site, insertion rates in HAP1 ΔMLH1 cells are as correlated to HEK293T cells as

182   replicates (Pearson's R = 0.88, Figure 2e, Supplementary Figure 1b) while correlations

183   between wild type HAP1 and HAP1 ΔMLH1 cells are modest (Pearson's R = 0.35, Figure 2f)

184   and improve when stratifying by sequence length. The same pattern of higher insertion rates

185   for short sequences in ΔMLH1 cells was observed for the FANCF locus (Supplementary

186   Figure 2f,g). These findings highlight that MMR proficiency is the major source of variation

187   between the tested cellular contexts for prime insertions.

Sequence effects

189   We next examined the length-independent causes of variation in insertion rate. We calculated

190   the relative insertion rate for each insert by dividing its marginal rate by the median in a 5-nt

191   length bin (Methods), and observed it is positively correlated with GC content across all target

192   sites and cell lines (Figure 3a). Each extra percentage in GC content increased the relative

193   insertion rate between 1.8% (FANCF site in HEK293 cells) and 4.9% (EMX1 site HEK293T

194   cells) on average. Specifically, we observed a strong cytosine preference for the CLYBL,

195   EMX1, and HEK3 loci (each extra percent cytosine increases relative insertion rate by 2.7-

196   5.4%), while both the percent of cytosines (0.9-1.2%) and guanines (1.3-3.3%) increase

197   insertion rates for the FANCF locus. Conversely, percent of adenine and thymine decreased

198   insertion rates for all loci and cell lines (-0.8% to -5.1% and -0.5% to -3.6% respectively,

199   Supplementary Figure 3a,b).
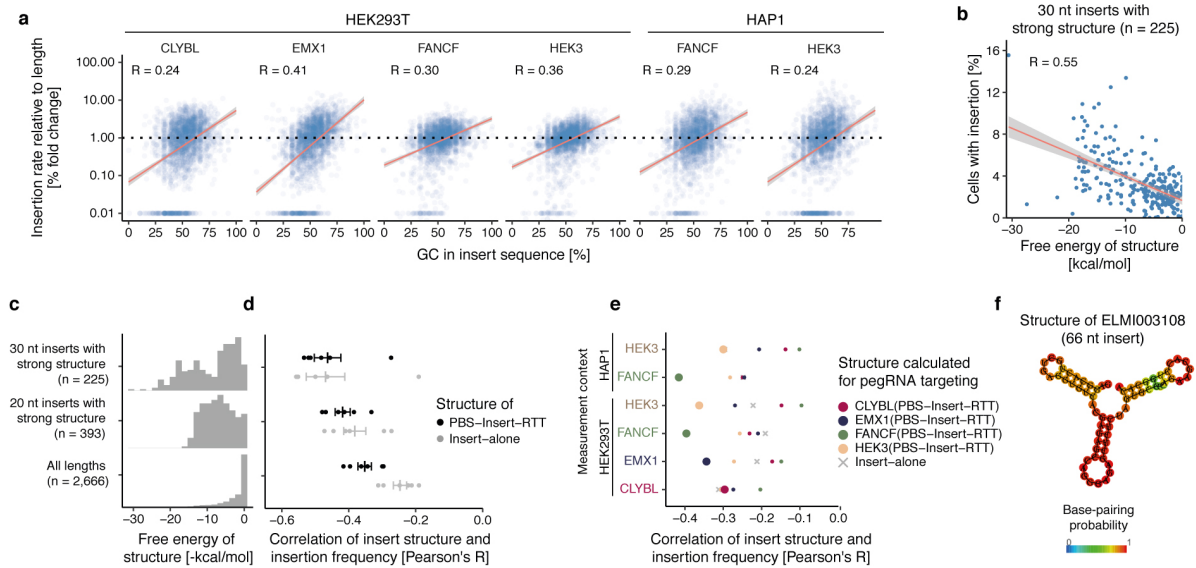
Figure 3. GC content and secondary structure of the insert sequence are positively correlated with insertion rate. a. Insertion efficiency dependence on GC content. Insertion rate relative to length bin average (y-axis) for inserts with different GC content (x-axis) of individual sequences (markers) at different target sites and cell lines (panels). Red line: linear regression fit; shaded area: 95% posterior confidence interval of the fit. Data represent the average of n=3 biological replicates. **b.** Insert sequence free energy correlation with insertion rate. Percent of cells with insertion (y-axis) for 30 nt sequences in the HEK3 locus in HEK293T cells (markers) with calculated Gibbs free energy (ΔG) from ViennaFold (x-axis). Red line: linear regression fit; shaded area: 95% posterior confidence interval of the fit. Data represent the average of n=3 biological replicates. **c.** Subsets of insertion sequences with fixed length and variable secondary structure. Frequency (y-axis) of insert sequence free energy (ΔG, x-axis) for 30 nt (top panel) and 20 nt sequences (middle panel), and the entire library (bottom panel). **d.** Correlation of insertion frequency and insert structure ΔG (x-axis) for 30 and 20 nt sequences, and the entire library (y-axis), stratified by whether ΔG was calculated for the insert sequence alone (grey) or for the entire 3'-extension, consisting of primer binding site (PBS), insert, and reverse transcription template (RTT; black) for different combinations of target sites and cell lines (markers). Data represents averages from n=3 biological replicates. Bars: mean and standard error of the mean. **e.** Target dependence of pegRNA secondary structure free energy correlation to insertion rate. Correlation (x-axis) between insertion efficiency measured in different target sites and cell lines (y-axis) and pegRNA 3' extension structure free energy calculated for pegRNAs against different target sites (colored markers), as well as insert sequence alone (grey cross). **f.** Example long sequence with successful insertions. The predicted secondary structure of a 66 nt insert sequence (ELMI003108) which was inserted with 1.4% efficiency into the HEK3 locus in HEK293T cells. Colors: base pairing probability.

225 Our library contained 225 and 291 insert sequences of 20 nt and 30 nt respectively, that were
226 designed to form secondary structures of varying strength, including some sequences with
227 perfect hairpins. Their secondary structure free energy as quantified by the Vienna fold ΔG
228 (more negative ΔG values indicate stronger secondary structures)[31,32] was negatively
229 correlated with insertion efficiency (average Pearson's R = -0.38 and -0.50 for 20 nt and 30 nt
230 insertions respectively, Figure 3b-d, Supplementary Figure 3c). Even when excluding the
231 shortest inserts of up to 3 nt, most of the inserted sequences in the library do not form strong
232 structures (Figure 3c) and the Vienna fold free energy explains less signal variation (average
233 Pearson's R=-0.25). We speculated that more important than the structure of the insert
234 sequence alone is the structure across the entire pegRNA 3' extension, comprising the primer
235 binding site and the reverse transcription template, and indeed, more variation was explained
236 when including the extension (average Pearson's R=-0.35, Figure 3d, Supplementary Figure
237 3d-f). Since the extension is specific to the target, this partly explains the differences in
238 insertion rates we observed across target sites. To quantify this effect, we measured how well
239 free energies of pegRNA extensions designed for one target site predict insertion efficiency at
240 another target site. Consistent with a target site-specific effect, the correlation was strongest
241 when the target site was matching to the 3' extension the structure it was calculated from
242 (Figure 3e).

243

244 Combining insert sequence length, GC content and structure explained why some sequences
245 inserted much better than others, which can help guide the choice of tags to insert. For
246 example, the long 66 nt ELMI003108 sequence that was inserted in the HEK3 locus at 1.39%
247 insertion frequency (0.66% on average for the other 10 sequences > 66 nt) had a GC content
248 of 62% and formed a strong structure alone as well as within the pegRNA context (ViennaFold
249 free energy = -23.8 and -37.5 respectively, Figure 3f). Other longer sequences that inserted
250 well relative to their size were recombinase sites, presumably due to their secondary structure
251 that often contains hairpins (Supplementary Figure 4a,b).

252 **CRISPR system effects**

253 Finally, we considered how aspects of the CRISPR/Cas system itself impact insertion rates.
254 First, it is known that the occurrence of four consecutive thymines acts as a transcription
255 terminator for RNA polymerase III and strongly impairs guide RNA expression[33,34]. We
256 confirmed that the average insertion rate for sequences that contain this tetranucleotide was
257 4.2 to 11.6-fold lower compared to sequences without (Figure 5a), while stretches of four
258 adenines showed a weaker but significant effect (average 1.5 to 1.8-fold reduction,

259   Supplementary Figure 4c). Overall, 21 of the 24 pegRNAs that were not inserted in any screen

260   contained at least one instance of the TTTT sequence.

261

262   Second, to disentangle the contribution of the reverse transcription step, we made a prime

263   editor construct with the nicking Cas9 fused to an engineered feline leukemia virus reverse

264   transcriptase (MashUp RT - pipettejockey.com) with a similar fidelity to the murine leukemia

265   virus RT used in PE2. The average insertion rates observed using this construct were 4.6-fold

266   lower compared to the standard PE2 (0.98% and 4.56% respectively; Figure 4b), but as

267   correlated to PE2 as another biological replicate (Pearson's R=0.80; Figure 4c, Figure 1e),

268   and with consistent marginal effects of the contributing features (Supplementary Figure 5).

269   Therefore, the reverse transcriptase used is not a major cause of variation in insertion rate in

270   our study.

271

272   Including an additional sgRNA to nick the non-edited strand increases editing efficiency as

273   well as indel formation rate[12]. We next explored how the addition of this extra sgRNA affects

274   the insertion frequencies of our library. We chose the EMX1 locus in HEK293T cells where we

275   observed poor insertion efficiencies of 0.28% on average without the nicking guide RNA, and

276   co-transfected with a nicking guide RNA that targets 77 nt downstream of the pegRNA target[35].

277   We found that the extra nick increased the average insertion rate by 5.7-fold to 1.59%, and

278   moderately increased the indel rate by 1.7-fold to 0.22% (Figure 4b). Importantly, the relative

279   insertion rates for sequences in the library remained similar, with correlations in line with those

280   of biological replicates and the other reverse transcriptase (Pearson's R=0.84, Figure 4d), and

281   consistent feature impact (Supplementary Figure 5) suggesting the determinants of prime

282   insertion efficiency we uncovered for PE2 are also valid for PE3.

283
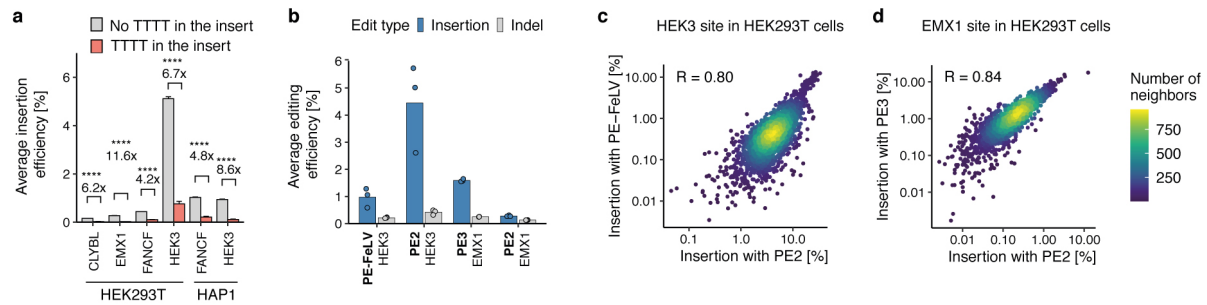
Figure 4. CRISPR system effects. a. Impact of four consecutive thymines. Average insertion rate (y-axis) for different screens (x-axis) stratified by presence of four consecutive thymines (grey: absent; red: present). Comparison: ratio of grey to red bar height. p-values derived from a two-sided student's t-test with all p-values $< 1\times10^{-67}$. n=3 biological replicates. **b.** Editing frequencies for alternative prime editing systems. Mutation frequency (y-axis) for three biological replicate screens (markers) using different prime editor systems (x-axis) stratified by mutation type (blue: insertions; grey: indels). Bar: average of markers. **c.** Impact of an alternative reverse transcriptase. Insertion frequencies at the HEK3 site in HEK293T using the standard MMLV reverse transcriptase (PE2, x-axis) and the FeLV reverse transcriptase (PE-FeLV, y-axis) for different insertion sequences (markers). Colors: number of neighboring data points. Label: Pearson's R. n=3 biological replicates **d.** As c), but comparing PE3, and at EMX1 site.

Predicting insertion rates

Given our improved understanding of prime insertion efficiency, we next created a prediction model. We extracted salient features such as insert length, nucleotide composition, and folding energy for each pegRNA, and trained regression models of insertion rates. We chose to use XGBoost (gradient boosted decision trees[36]), as it achieved the best cross-validation performance (Figure 5a), and further evaluated its accuracy on datasets narrowed to individual sites and cell lines (Supplementary Figure 6a). The model generalized well (Supplementary Figure 6b), but we noticed that training on data only from HAP1 experiments resulted in worse performance on the HEK293T and HAP1 ΔMLH1 lines (average Pearson's R = 0.31 vs 0.49 and 0.50 respectively). Given the observations of mismatch repair importance above, and the lack of repair proficiency as a feature input to the model, we hypothesized that including an experiment-specific and sequence-independent feature to capture this will improve prediction accuracy. Indeed, the model improved substantially when adding MMR status as a feature (increase in Pearson's R > 0.1; paired t-test $p < 10^{-3}$; Figure 5b).
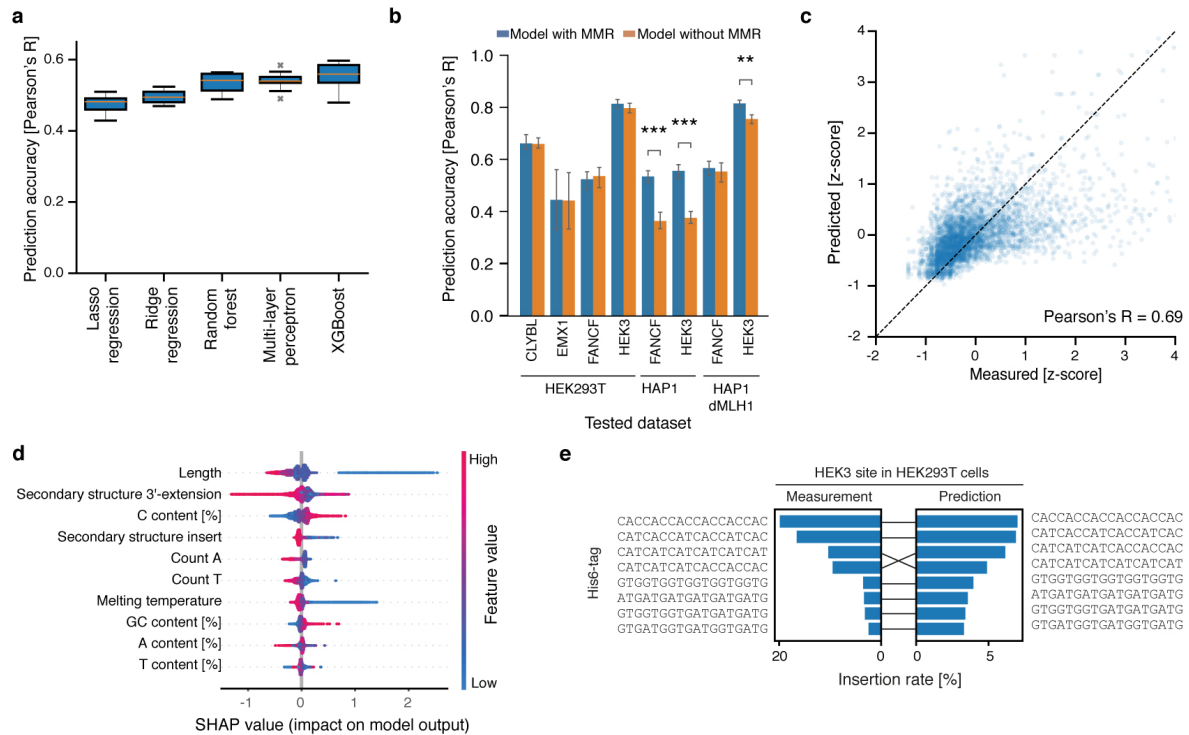
11

Figure 5. Predicting prime insertion efficiencies. a. Cross-validation performance of different models. Pearson's R between predicted and measured held-out pegRNAs (y-axis) for ten cross-validation folds across a range of models (x-axis). Box: median and quartiles; whiskers: 90th percentile; cross: outlier. **b.** Impact of sequence-independent mismatch repair (MMR) proficiency feature. Pearson's R between measured and predicted insertion rate on held-out pegRNAs (y-axis) on different screens (x-axis) for XGBoost model that includes MMR feature (blue) or not (orange). Whiskers: standard error of mean. Comparison: Student's t-test between models with MMR and without; ***: $p < 10^{-3}$; **: $p < 10^{-2}$. **c.** Concordance of prediction and measurement. Predicted (x-axis) and measured (y-axis) insertion efficiency on the combined dataset for held-out pegRNAs (markers). Label: Pearson's R. Dashed line: y=x. **d.** Feature importance. Distribution (row y-axis) of SHAP values (x-axis) for features ordered top to bottom by median absolute SHAP value (y-axis). Colors: feature value. **e.** His6-tag insertion rate. Insertion rate (x-axis) for Predicted (right) vs. measured (left) insertion rates of different alternative His6-tags (y-axis) into HEK3 locus in HEK293T cells.

Our final model is trained on data from experiments on all cell lines and target sites, and includes sequence characteristics as well as repair proficiency as features. It predicted insertion rates for unseen insert sequences with high accuracy (Pearson's R=0.69, Figure 5c), which is very near the limit set by the correlation of biological replicates (average Pearson's R=0.76). The features important for prediction[37] reflected the observations above, with insert sequence length, secondary structure of the pegRNA, and nucleotide composition having the largest impact (Figure 5d). We call this method MinsePIE (Modelling insertion efficiency for

334   Prime   Insertion   Experiments)   and   make   it   available   at

335   https://github.com/julianeweller/MinsePIE.

336

337   Predictive models inform experiments and help in selecting the components of a desired

338   insertion. A common application of small sequence insertion is endogenous protein tagging,

339   and the His6-tag is frequently used to enable purification. The possible tags that give

340   equivalent amino acid sequences range in codon choice, thus resulting in pegRNAs with

341   varying secondary structure and nucleotide composition when inserted. Our library contained

342   8 codon variations of the His6-tag in forward and reverse orientations. The average insertion

343   difference between the best codon variant and the worst was 13.3-fold, highlighting the

344   importance of choosing the optimal codon variant for insertion. We withheld the data for all

345   His6-tags in our library from the training set, and predicted their efficacy of insertion into the

346   HEK3 locus in HEK293T cells. The versions of the His6-tag that were both predicted and

347   measured to have the highest insertion rates had the highest cytosine content by using mainly

348   the CAC histidine codon (Figure 5e). While the predicted preference varied across target

349   contexts, the His6-tag with the highest predicted insertion rate was within the top two

350   measured rates in each editing context (Supplementary Figure 6).

DISCUSSION

352   We present the first comprehensive analysis of prime editing insertion efficiencies using 2,666

353   pegRNAs. We discovered that short sequences insert with predictable frequencies across cell

354   lines, target sites, and prime editor systems based on their length, GC content and tendency

355   to form secondary structure. Together, these features enable it to accurately predict variation

356   in insertion rates, and to choose optimal reagents for writing short stretches of DNA into

357   genomes.

358

359   We uncovered a complex relation between insertion sequence length and efficiency.

360   Sequences between 15 and 21 nt generally inserted well, while longer sequences are

361   incorporated less frequently, but still at moderate efficiencies even for sequences larger than

362   60 nt. This disparity is potentially due to steric issues for reverse transcription and base pairing

363   with the unedited strand. The insertion efficiency of sequences shorter than 10 nt was variable,

364   with high rates in MMR-deficient cell lines (HEK293T, HAP1 ΔMLH1) but not in MMR-proficient

365   ones (HAP1). This is consistent with recent findings that MMR antagonizes prime editing[17].

366   Longer sequences are less efficiently recognized by MMR[30] and therefore insert better than

367   short ones in mismatch repair proficient cell lines.

368   We further discovered that stronger secondary structure of the pegRNA 3'-extension led to

369   higher insertion efficiency. This effect was evident when comparing different inserts into the

370   same target, but also explained variable rates when attempting to write the same sequence

371   into different target sites. One potential explanation is that structured pegRNAs are more

372   protected from digestion by 3'-exonucleases. Indeed, Nelson and Randolph *et. al.* recently

373   demonstrated that incorporating structured motifs at the 3'-end of pegRNAs improved prime

374   editing efficiency 3 to 4-fold by preventing degradation of the 3'-extension[18]. Alternatively,

375   structured inserts could ease pairing of the edited strand with the non-edited strand due to

376   being sterically smaller via folding onto themselves.

377

378   Our improved understanding of insertion efficiency using the prime editing system naturally

379   leads to recommendations for experimental design. First, we suggest choosing sequences

380   with high GC, and especially cytosine content that are prone to form secondary structures.

381   Sequences whose lengths vary between 15 and 21 nt are well inserted using prime editing

382   while sequences between 10 and 14 nt are not. Knocking out MLH1 will drastically improve

383   insertion rates for sequences shorter than 10 nt. To boost the efficiency of short sequence

384   insertions in mismatch repair proficient contexts, additional silent mutations should be inserted

385   on the reverse transcriptase template or mismatch repair could be transiently inhibited (as

386   implemented in PE4 or PE5 systems)[17].

387

388   These factors can influence the choice of tag and codon. For example, the His-6 tag,

389   especially if choosing the CAC codon, inserts almost 6 times as well as the next best tag in

390   our library (Myc-tag). For the correction of pathogenic deletions, our model can help prioritize

391   targets and pick high efficiency replacement sequences (for example through codon variation).

392   Our libraries cover many commonly used small sequences and their respective insertion

393   efficiencies (Supplementary Data 2). For predicting the insertion efficiency of novel

394   sequences, we provide the MinsePIE algorithm as a command line script.

395

396   We studied four target sites in two cell lines across three prime editor systems and uncovered

397   both universal and target site-dependent determinants of insertion efficiency. Models trained

398   specifically on one target site still outperformed predictions on withheld data from the same

399   target site when compared to predictions on other target sites. Screening a smaller focussed

400   library across many target sites should help to more fully understand the interactions of target

401   site and insertion sequences. Moreover, all pegRNAs had a constant primer binding site length

402   of 13 nt and a reverse transcriptase template length (without insertion) of 34 nt. Given the

403 model based on our sequence features (that implicitly also quantify these factors) generalised
404 well to unseen pegRNAs, we expect the determinants we uncovered to also broadly hold for
405 different lengths of primer binding site and reverse transcriptase template.
406
407 The prime editing field is moving rapidly[38]. Diverse applications are already emerging[39] and
408 some of the most exciting ones are specifically built around insertion of short sequences.
409 Communicated, but as yet unpublished examples include insertion of recombinase sites using
410 prime editing to enable directed insertion of large DNA cargo of up to 36 kb[1,2], as well as clever
411 utilization of short sequence insertion to generate a molecular recorder for sequential cellular
412 events[40-42]. Better understanding of how cellular determinants[17] and pegRNA features affect
413 prime editing rates[14,18] provides a foundation for these advances. Our work adds the important
414 dimension of short sequences insertions, which hold the promise to both enable sophisticated
415 genome engineering and to correct thousands of pathogenic mutations.

Author contributions

417 Conceptualized and initiated the study: JK, LP. Performed experiments: EMP with help from:
418 JK, FL. Analysed the data: JK, JW with help from: AP. Build the machine learning models: JW
419 with help from: AP. Supervised the project: LP with help from: FL. Wrote the manuscript: JK,
420 JW, LP with input from all authors.

Competing interests

422 The authors do not declare any competing interests

Acknowledgements

METHODS

Mammalian cell culture

The human HEK293T cell line was purchased from AMS Biotechnology (EP-CL-0005). The HAP1 WT cell line was provided by Andrew Waters (Wellcome Sanger Institute) and the HAP1 ΔMLH1 cell line was purchased from Horizon discovery (HZGHC000343c022). HEK293T cells were cultured in DMEM (Invitrogen) and HAP1 cells in IMDM (Invitrogen), both supplemented with 10% FCS (Invitrogen), 2 mM glutamine (Invitrogen), 100 U/ml penicillin and 100 mg/ml streptomycin (Invitrogen) at 37 °C and 5% CO_2.

Primers

All primers used in this study are listed in Supplementary Table 1.

Library design

The insert sequence library contained 2,666 sequences, made up from useful molecular biology sequences, the eukaryotic motif library (ELM) and sequences with strong secondary structure. The utility sequences were hand-picked for their usefulness in molecular biology. The ELM instances library with the corresponding fasta file of the genes was downloaded from elm.eu.org/instances.html?q=*[26,27] on 2020/11/19 and filtered to only contain sequences from "homo sapiens" that are longer than 1 amino acid. The amino acid motifs were extracted from the fasta file based on the indicated start and end sites. Finally, the amino acid motifs were reverse translated into DNA sequence using the 'reversetranslate' R package (version 1.0.0) and using the most frequent codon from the homo sapiens codon table. For the secondary structure library, 100,000 random DNA sequences of 20 and 30 nt length were generated (RBioinf::randDNA function; version 1.48.0) and their secondary structure calculated (see insert sequence structure section). The sequences were distributed into 10 bins based on the strength of their secondary structure and 20 sequences were randomly picked from each structure bin to be included in the library. Finally, 30 random perfect 20 and 30 nt RNA hairpins were generated and amended to the secondary structure library. The combined library of insert sequences is included as Supplementary Data 1. The insert sequences were then flanked with primer binding sites, random nucleotide stuffer sequence for shorter inserts, BsmBI sites and target vector compatible overhangs, resulting in 11,166 sequences of 199 nt (Supplementary Data 3). The oligonucleotide library was ordered from Twist Biosciences.

Plasmid cloning

16

466 *pCMV-PE2-P2A-PuroR* was generated by replacing eGFP from pCMV-PE2-P2A-GFP
467 (Addgene 132776) with PuroR. Therefore, a gene fragment containing parts of the MMLV
468 reverse transcriptase and the puromycin resistance gene was ordered from IDT
469 (Supplementary Table 3). The gene fragment and pCMV-PE2-P2A-GFP were digested using
470 AgeI, purified with the Monarch PCR & DNA Cleanup Kit (NEB) and ligated with T4 DNA ligase
471 (NEB). 2 µl of the ligation product was transformed into bacteria using XL10-Gold
472 Ultracompetent Cells (Agilent) according to the manufacturer's protocol. Plasmid DNA was
473 isolated using the Plasmid Plus Midi Kit (Qiagen).

474

475 *pCMV-PE-FeLV-P2A-EGFP* was generated by replacing the MMLV coding sequence
476 between the XTEN linker and the 2A cleavage peptide with a synthesised gene fragment from
477 IDT using Gibson Assembly that encodes an IDT human codon optimised version of the
478 MashUp reverse transcriptase (pipettejockey.com) that is engineered from the Feline
479 Leukaemia Virus (UniProt Q85521).

480

481 *pLentiGuide-Blast* was generated by replacing the puromycin resistance gene from
482 Lenti_gRNA-Puro (Addgene 84752) with a blasticidin resistance gene. A gene fragment
483 containing parts of the EF1a promoter and the blasticidin resistance gene was ordered from
484 Twist Biosciences (Supplementary Table 3). The gene fragment and Lenti_gRNA-Puro were
485 digested using FseI (NEB) and MluI-HF (NEB), purified with the Monarch PCR & DNA Cleanup
486 Kit (NEB) and ligated with T4 DNA ligase (NEB). 2 µl of the ligation product was transformed
487 into bacteria using XL10-Gold Ultracompetent Cells (Agilent) according to the manufacturer's
488 protocol. Plasmid DNA was isolated using the Qiagen Spin Miniprep Kit.

489

490 **Library cloning**

491 First, a separate, site-specific backbone was cloned for each target site. A gene fragment was
492 ordered containing the protospacer, guide RNA scaffold, parts of the reverse transcriptase
493 template and primer binding site, a stuffer sequence flanked with BsmBI sites for insert library
494 insertion and the T7 terminator motif (Supplementary table 3). 100 ng of the gene fragments
495 were digested with BsaI-HFv2 (NEB) and purified with the Monarch PCR & DNA Cleanup Kit
496 (NEB). The pLentiGuide-Blast plasmid was digested with BsmBI-V2 (NEB) at 55°C for 8h
497 followed by 20 min heat inactivation at 80°C and gel purified using the QIAEX II Gel Extraction
498 Kit (Qiagen). The gene fragments were ligated into the backbone using T4 DNA ligase (NEB)
499 and transformed into XL10-Gold Ultracompetent bacteria (Agilent). The plasmids were purified
500 with Qiagen Spin Miniprep Kit.

501

502 Second, pegRNA insert libraries were inserted into the site-specific backbones. The insert

503 libraries were synthesized as 199 nt oligo pools (Twist BioSciences) and amplified using KAPA

504 HiFi HotStart ReadyMix (Roche). Libraries for individual target sites were amplified with

505 separate primers (Supplementary Table 1). The products were purified using the Monarch

506 PCR & DNA Cleanup Kit, digested with BsmBI-v2 at 55°C for 4h and heat inactivated at 80°C

507 for 20 min alongside 5 µg of site-specific plasmids. The digested oligos were purified using

508 the Monarch PCR & DNA Cleanup Kit. The vectors were treated with quick CIP (NEB) for 15

509 minutes at 37°C and then purified using QIAquick PCR Purification Kit (Qiagen). Inserts were

510 ligated into vectors using Golden Gate assembly. A 1:3 molar ratio of insert and vector were

511 mixed with BsmBI-v2 and T4 DNA ligase and incubated in a thermocycler for 30 cycles,

512 alternating between 5 minutes at 42°C and 5 min at 16°C and finishing with a heat inactivation

513 step at 60°C for 5 min. The ligation products were purified with Monarch PCR & DNA Cleanup

514 Kit and electroporated into MegaX DH10B T1R Electrocomp Cells (Thermo Fisher) according

515 to manufacturer's protocol. The bacteria were grown overnight in liquid culture and plasmid

516 was extracted using the Plasmid Plus Midi Kit. The spacer sequences, primer binding sites,

517 and reverse transcriptase templates (without insertions) are attached as Supplementary

518 Table 2).

519

520 **Lentivirus production**

521 Lentivirus was produced in HEK293FT cells that were transfected with Lipofectamine LTX

522 (Invitrogen). 5.4 µg of a lentiviral vector, 5.4 µg of psPax2 (Addgene 12260), 1.2 µg of pMD2.G

523 (Addgene 12259) were mixed in 3 ml Opti-MEM together with 12 µl PLUS reagent and

524 incubated for 5 min at room temperature. 36 µl of the LTX reagent was added and the mix

525 was incubated for another 30 min at room temperature. 3 ml of the transfection mix was then

526 added to 80% confluent cells in 10 ml DMEM media in a 10-cm dish. After 48h the supernatant

527 was collected and stored at 4°C. Fresh media was added to the cells and harvested 24h later.

528 The two harvests were kept separate. For virus titration, Lenti-X GoStix Plus (Takara) was

529 used following the manufacturer's protocol.

530

531 **pegRNA insertion screens**

532 *Infection with pegRNA library.* All cell lines were infected with the pegRNA library aiming at a

533 multiplicity of infection (MOI) of 0.5 and a guide coverage of > 1000x. Each screen was

534 performed in 3 biological replicates and independently infected. To achieve this, 6×10^6 cells

535 were plated in three wells of a six well plate and spin infected for 15-30 mins at 2000 rpm.

536 Following infection, cells were resuspended and replated at $2\text{x}10^4$ cells/cm². Cells were

537 cultured for 7 days and selected for pegRNA integration with 10 μg/ml blasticidin. Cells were

538 passaged at day 3 post-infection and a higher coverage than at the time of infection was

539 maintained.

540

541 *Transfection with prime editors.* HEK293T cells were seeded at a concentration $6.9\text{x}10^4$

542 cells/cm² to a 15-cm dish. The next day the media was replaced with fresh media and the cells

543 were transfected using Lipofectamine LTX reagent. Next, 72 μg PE-Puro or PE-FeLV plasmid

544 were mixed with 8 μg pCS2-GFP and 40 μl Lipofectamine P3000 (Invitrogen) in 3.2 ml Opti-

545 Mem (Gibco). In another tube, 40 μl of Lipofectamine 3000 and 160 μl Lipofectamine LTX

546 were mixed in 3.2 ml Opti-Mem. The solutions were mixed together, incubated for 30 minutes

547 at room temperature and then added onto the cells. For PE3, an additional 6 μg of nicking

548 guide RNA was added.

549

550 Hap1 and HAP1 ΔMLH1 cells were seeded at a concentration of $9.3\text{x}10^4$ cells/cm² into two

551 T75-flasks. The following day, the media was refreshed one hour before transfection. Cells

552 were transfected using Xfect Transfection Reagent (Takara). Next, 72 μg PE-Puro plasmid

553 was mixed with 8 μg pCS2-GFP and Xfect Reaction Buffer to a total volume of 750 μl. To the

554 reaction, 48 μl of I Xfect Polymer was added and incubated at room temperature for 10

555 minutes. The mixture was then added onto the cells. Media was changed 4 h after transfection.

556 One day after transfections, 2 μg/ml of puromycin was added to the cells to start selection.

557 Cells were kept in selection for 3 days and harvested 5 days after transfection.

558

559 **DNA extraction and library preparation for next generation sequencing**

560 Genomic DNA extraction and sequencing library preparation for screens were done as

561 described in Allen et al., 2019[10]. Briefly, cell pellets were resuspended in TAIL BUFFER A

562 (100 mM Tris-HCl, 5 mM EDTA, 200 mM NaCl) and then mixed with 1 volume of TAIL BUFFER

563 B (100 mM Tris-HCl, 5 mM EDTA, 200 mM NaCl, 0.4% SDS) supplemented with freshly

564 thawed Proteinase K (20 mg/ml final). The lysate was incubated overnight at 56˚C. On the

565 next day, RNase A was added to a final concentration of 10 μg/ml and incubated at 37˚C for

566 30 min - 4 h. 1 volume of isopropanol was added and the DNA spooled on a sterile inoculation

567 loop. The DNA was washed three times by dipping into consecutive 5 ml tubes containing

568 70% ethanol. The DNA was air dried for 5-10 mins and resuspended in TE buffer (pH 8.0).

569

570   For each screen, two independent amplicons were generated by PCR using Q5 Hot Start

571   High-Fidelity 2X Master Mix (NEB). One amplicon for the targeted locus and one amplicon of

572   the pegRNA locus (primers listed in Supplementary Table 1, staggered forward primers were

573   used to ensure complexity for sequencing). To ensure coverage for each sample, 40 μg of

574   gDNA was used as template and each PCR reaction was run in 50 μl aliquots containing no

575   more than 5 μg DNA. The PCR reactions were column-purified using the QIAquick PCR

576   Purification Kit (Qiagen). Sequencing adaptors and barcodes were added with a second round

577   of PCR using the KAPA HiFi HotStart ReadyMix (Roche), primers P3 and P4 (Supplementary

578   Table 1) and 1 ng of template DNA. Amplicons were purified with Agencourt AMPure XP beads

579   in 0.7:1 ratio (beads to PCR reaction volume) and quantified with the Quant-iT™ High-

580   Sensitivity dsDNA Assay Kit (Invitrogen). The amplicons were pooled together and sequenced

581   on the Illumina HiSeq 2500 using HiSeq Rapid SBS Kit v2 (500 cycles, no phiX addition).

582

583   **Generating read count tables**

584   Paired forward and reverse reads from illumina sequencing were merged using PEAR v0.9.11.

585   Data for the same screen but from different sequencing lanes was concatenated. The resulting

586   merged fastq files were processed using a custom R script (read_match_pegRNAs.R in

587   Supplementary Information). First, DNA sequences were trimmed to contain the 10 nt up and

588   downstream of the nick site (for target site amplicon) or to contain 15 nt up and downstream

589   of the nick site (pegRNA amplicon). On average, 98% of reads were matched for the target

590   site amplicon and 84% for the pegRNA amplicon. The trimmed sequences were then matched

591   to each insert in the pegRNA library in the context of 10 nt target site (for target site amplicon)

592   or in the context of 15 nt pegRNA plasmid (pegRNA amplicon), requiring 0 mismatches.

593   Adding the context is to ensure that only insertions at the correct location are considered. On

594   average 92% of reads were matched to the unedited locus or an insertion for both the target

595   site amplicon and the pegRNA amplicon. The read count tables are attached as

596   Supplementary Data 2.

597

598   **Combining replicates**

599   We filtered out pegRNAs where any replicate had fewer than 10 reads in the pegRNA

600   amplicon mapping to it. Across the screens, between 39 and 174 pegRNAs did not pass this

601   minimum requirement, and were discarded from further analysis (1.5-6.5%, Supplementary

602   Figure 1d). pegRNA abundance in the screens correlated with their abundance in the plasmid

603   library (range of Pearson's R across all samples 0.84 to 0.96, Supplementary Figure 1e). Insert

604   counts were normalized to frequencies by dividing the reads for each insert by the number of

605 reads in each screen. Insertion efficiencies were calculated for each replicate and screen by

606 dividing the target insert frequency by the pegRNA insert frequency. Finally, insertion

607 efficiencies were averaged across replicates. The script used to combine replicates is

608 attached in the supplementary information as 'combine_replicates.R'. Insertion efficiencies

609 were normalized (z-score) between screens and replicates by subtracting the corresponding

610 mean insertion efficiency from each individual insertion efficiency and dividing it by the

611 standard deviation of the insertion efficiency.

612

613 **Mutation rates around the insertion site and indel detection**

614 The fastq reads of the target sites were trimmed by matching a stretch of ten nucleotides 60

615 nt up and downstream of the nicking site (CLYBL: TAGGGCTGGA, CAGAGTTCCA; EMX1:

616 GAGGACAAAG, ATGGGGAGGA; FANCF: GTCTCCAAGG, AGCACCTGGG; HEK3:

617 CTTTTTTTCT, AGCTTTTCCT). Occurrence of library insertions was detected by pattern

618 matching the trimmed reads for library sequences. Going from outside to inside (with the

619 nicking site being between the two innermost nucleotides), the occurrence of the four

620 nucleotides was counted at every position. There is a non-reference SNP (G>A) in HEK293T

621 cells for 2 of 3 alleles at position +9. The RT template on the pegRNA corresponds to the

622 sequence of the minor allele (A). For indel detection, the trimmed reads were filtered in a

623 series of steps. First, sequences with insertions at the nick site that perfectly match a

624 sequence in the insert libraries were removed (this also means that our method cannot detect

625 single/double/triple nucleotide insertions at the nick site because our library contains all

626 possible singlets/doublets/triplets). Second, sequences which contained 'N' were removed.

627 Third, sequences with a perfectly preserved sequence around the cut site were removed.

628 Fourth, sequences that are 120 nt long were removed (120 nt corresponds to the length of a

629 sequence without indels). The remaining sequences were classified as indels. The scripts

630 used to call mutation rates and indels are attached in the Supplementary Information as

631 'find_SNVs.R' and 'find_indels.R'.

632

633 **Data analysis**

634 Length residuals were calculated by dividing sequences into length bins and dividing the

635 insertion rate by the median insertion rate across the length bin. The length bins consisted of

636 sequences from 1-4, 5-9, 10-14, 30-39, 40-49, 50-59, and 60-69. The sequences with lengths

637 above 30 nt were divided into length bins of 10 nt because there were fewer longer sequences

638 in the library. Melting temperature for the insert sequence was calculated using

639 SeqUtils.MeltingTemp.Tm_NN from biopython. The Vienna fold (VF) algorithm[31,32] was used

21

640   to calculate the tendency of insert sequences to form secondary structures. RNA fold (version

641   2.4.16) was run on the insert sequences alone or on the insert sequences in context of the 13

642   nt PBS and 34 nt RT template with the --noPS parameter.

643

644   **Modelling**

645   Categorical features were one-hot encoded. Scikit-learn models were applied using default

646   parameters, if not stated otherwise. Lasso regression was performed with alpha = 0.1; Ridge

647   regression was performed with alpha of 0.03 and Stochastic Average Gradient descent;

648   Random forest had a maximum depth of 4 and 100 estimators; Multilayer perceptron regressor

649   with 100 hidden layers was trained with 500 maximum iterations at a constant learning rate of

650   0.001 and 'lbfgs' solver. Gradient boosted tree from XGBoost[36] was trained with a minimum

651   loss reduction of 0.1, 100 trees, a learning rate of 0.1, maximum depth of 5, no L1

652   regularization on weights, 0.375 L2 regularization on weights, and a 0.95 subsample ratio of

653   columns when constructing each tree. For training, unique insert sequences were split

654   randomly into training and test sequences at a ratio of 0.8. Measurements for different target

655   sites and cell lines were assigned into training and test data based on the grouping of insert

656   sequences. For 10-fold cross validation, insert sequences were split randomly for every fold

657   validation. The model was trained and predictions were evaluated using Pearson's R based

658   on the correlation between test data and corresponding predictions. SHapley Additive

659   exPlanations (SHAP) values for the model and feature importance for the prediction of specific

660   outcomes were calculated using the SHAP TreeExplainer and explainerModel[37].

661

662   **Statistics and reproducibility**

663   The *n* numbers denoted in the figure legends refer to independent experiments that were

664   separately infected with the pegRNA library. No statistical methods were used to predetermine

665   sample size. The experiments were not randomized and the investigators were not blinded to

666   allocation during experiments and outcome assessment.

667

668   **Data and material availability**

669   Read count tables for all screens, mutation frequencies at each position, sequences with

670   indels and scripts necessary to reproduce the analysis are attached in the Supplementary

671   Information. The pCMV-PE2-P2A-PuroR and pLentiGuide_BlastR plasmids will be made

672   available on AddGene. Scripts and models are made available on

673   https://github.com/julianeweller/MinsePIE.

674

Software

PEAR (0.9.11); Python (3.8.10); Python packages: Biopython (1.79), scikit-learn (0.24.2), scipy (1.5.3), shap (0.39.0), statannot (0.2.3), XGBoost (1.4.0); R (4.0.2); RNA fold (2.4.16); R packages: Broom (0.7.9), ggpointdensity (0.1.0), RBioinf (1.48.0), reversetranslate (1.0.0), ShortRead (1.46.0), spgs (1.0-3), Tidyverse (1.3.1), Viridis (0.6.1).

REFERENCES

1   Anzalone, A. V. *et al.* Programmable large DNA deletion, replacement, integration, and inversion with twin prime editing and site-specific recombinases. *bioRxiv*, 2021.2011.2001.466790, doi:10.1101/2021.11.01.466790 (2021).

2   Ioannidi, E. I. *et al.* Drag-and-drop genome insertion without DNA cleavage with CRISPR-directed integrases. *bioRxiv*, 2021.2011.2001.466786, doi:10.1101/2021.11.01.466786 (2021).

3   Landrum, M. J. *et al.* ClinVar: public archive of interpretations of clinically relevant variants. *Nucleic Acids Res* **44**, D862-868, doi:10.1093/nar/gkv1222 (2016).

4   Landrum, M. J. *et al.* ClinVar: improving access to variant interpretations and supporting evidence. *Nucleic Acids Res* **46**, D1062-D1067, doi:10.1093/nar/gkx1153 (2018).

5   Geurts, M. H. *et al.* Evaluating CRISPR-based prime editing for cancer modeling and CFTR repair in organoids. *Life Sci Alliance* **4**, doi:10.26508/lsa.202000940 (2021).

6   Schene, I. F. *et al.* Prime editing for functional repair in patient-derived disease models. *Nat Commun* **11**, 5352, doi:10.1038/s41467-020-19136-7 (2020).

7   Drumm, M. L., Ziady, A. G. & Davis, P. B. Genetic variation and clinical heterogeneity in cystic fibrosis. *Annu Rev Pathol* **7**, 267-282, doi:10.1146/annurev-pathol-011811-120900 (2012).

8   Zielenski, J. & Tsui, L. C. Cystic fibrosis: genotypic and phenotypic variations. *Annu Rev Genet* **29**, 777-807, doi:10.1146/annurev.ge.29.120195.004021 (1995).

9   Leibowitz, M. L. *et al.* Chromothripsis as an on-target consequence of CRISPR-Cas9 genome editing. *Nat Genet* **53**, 895-905, doi:10.1038/s41588-021-00838-7 (2021).

10   Allen, F. *et al.* Predicting the mutations generated by repair of Cas9-induced double-strand breaks. *Nat Biotechnol*, doi:10.1038/nbt.4317 (2018).

11   Kosicki, M., Tomberg, K. & Bradley, A. Repair of double-strand breaks induced by CRISPR-Cas9 leads to large deletions and complex rearrangements. *Nat Biotechnol* **36**, 765-771, doi:10.1038/nbt.4192 (2018).

12   Anzalone, A. V. *et al.* Search-and-replace genome editing without double-strand breaks or donor DNA. *Nature* **576**, 149-157, doi:10.1038/s41586-019-1711-4 (2019).

13   Anzalone, A. V., Koblan, L. W. & Liu, D. R. Genome editing with CRISPR-Cas nucleases, base editors, transposases and prime editors. *Nat Biotechnol* **38**, 824-844, doi:10.1038/s41587-020-0561-9 (2020).

14   Kim, H. K. *et al.* Predicting the efficiency of prime editing guide RNAs in human cells. *Nat Biotechnol* **39**, 198-206, doi:10.1038/s41587-020-0677-y (2021).

15   Kweon, J. *et al.* Engineered prime editors with PAM flexibility. *Mol Ther* **29**, 2001-2007, doi:10.1016/j.ymthe.2021.02.022 (2021).

16   Liu, Y. *et al.* Efficient generation of mouse models with the prime editing system. *Cell Discov* **6**, 27, doi:10.1038/s41421-020-0165-z (2020).

17   Chen, P. J. *et al.* Enhanced prime editing systems by manipulating cellular determinants of editing outcomes. *Cell* **184**, 5635-5652 e5629, doi:10.1016/j.cell.2021.09.018 (2021).

18   Nelson, J. W. *et al.* Engineered pegRNAs improve prime editing efficiency. *Nat Biotechnol*, doi:10.1038/s41587-021-01039-7 (2021).

19   Doench, J. G. *et al.* Optimized sgRNA design to maximize activity and minimize off-target effects of CRISPR-Cas9. *Nat Biotechnol* **34**, 184-191, doi:10.1038/nbt.3437 (2016).

20   Meier, J. A., Zhang, F. & Sanjana, N. E. GUIDES: sgRNA design for loss-of-function screens. *Nat Methods* **14**, 831-832, doi:10.1038/nmeth.4423 (2017).

21   Kim, H. K. *et al.* SpCas9 activity prediction by DeepSpCas9, a deep learning-based model with high generalization performance. *Sci Adv* **5**, eaax9249, doi:10.1126/sciadv.aax9249 (2019).

22   Arbab, M. *et al.* Determinants of Base Editing Outcomes from Target Library Analysis and Machine Learning. *Cell* **182**, 463-480 e430, doi:10.1016/j.cell.2020.05.037 (2020).

23   Pallaseni, A. *et al.* Predicting base editing outcomes using position-specific sequence determinants. *bioRxiv*, 2021.2009.2016.460622, doi:10.1101/2021.09.16.460622 (2021).

24   Song, M. *et al.* Sequence-specific prediction of the efficiencies of adenine and cytosine base editors. *Nat Biotechnol* **38**, 1037-1043, doi:10.1038/s41587-020-0573-5 (2020).

25   Feng, S. *et al.* Improved split fluorescent proteins for endogenous protein labeling. *Nat Commun* **8**, 370, doi:10.1038/s41467-017-00494-8 (2017).

26   Dinkel, H. *et al.* The eukaryotic linear motif resource ELM: 10 years and counting. *Nucleic Acids Res* **42**, D259-266, doi:10.1093/nar/gkt1047 (2014).

27   Puntervoll, P. *et al.* ELM server: A new resource for investigating short functional sites in modular eukaryotic proteins. *Nucleic Acids Res* **31**, 3625-3630, doi:10.1093/nar/gkg545 (2003).

28   Cerbini, T. *et al.* Transcription activator-like effector nuclease (TALEN)-mediated CLYBL targeting enables enhanced transgene expression and one-step generation of dual reporter human induced pluripotent stem cell (iPSC) and neural stem cell (NSC) lines. *PLoS One* **10**, e0116032, doi:10.1371/journal.pone.0116032 (2015).

29   Trojan, J. *et al.* Functional analysis of hMLH1 variants and HNPCC-related mutations using a human expression system. *Gastroenterology* **122**, 211-219, doi:10.1053/gast.2002.30296 (2002).

30   Gupta, S., Gellert, M. & Yang, W. Mechanism of mismatch recognition revealed by human MutSbeta bound to unpaired DNA loops. *Nat Struct Mol Biol* **19**, 72-78, doi:10.1038/nsmb.2175 (2011).

31   Gruber, A. R., Lorenz, R., Bernhart, S. H., Neubock, R. & Hofacker, I. L. The Vienna RNA websuite. *Nucleic Acids Res* **36**, W70-74, doi:10.1093/nar/gkn188 (2008).

32   Hofacker, I. L. Vienna RNA secondary structure server. *Nucleic Acids Res* **31**, 3429-3431, doi:10.1093/nar/gkg599 (2003).

33   Chen, B. *et al.* Dynamic imaging of genomic loci in living human cells by an optimized CRISPR/Cas system. *Cell* **155**, 1479-1491, doi:10.1016/j.cell.2013.12.001 (2013).

| 765 | 34 | Porrua, O., Boudvillain, M. & Libri, D. Transcription Termination: Variations on Common Themes. *Trends Genet* **32**, 508-522, doi:10.1016/j.tig.2016.05.007 (2016). |

766

767   35   Liu, P. *et al.* Improved prime editors enable pathogenic allele correction and cancer
768   modelling in adult mice. *Nat Commun* **12**, 2121, doi:10.1038/s41467-021-22295-w
769   (2021).
770   36   Chen, T. & Guestrin, C. in *Proceedings of the 22nd ACM SIGKDD International*
771   *Conference on Knowledge Discovery and Data Mining*   785–794 (Association for
772   Computing Machinery, San Francisco, California, USA, 2016).
773   37   Lundberg, S. & Lee, S.-I. A Unified Approach to Interpreting Model Predictions.
774   arXiv:1705.07874 (2017).
775   <https://ui.adsabs.harvard.edu/abs/2017arXiv170507874L>.
776   38   Scholefield, J. & Harrison, P. T. Prime editing - an update on the field. *Gene Ther* **28**,
777   396-401, doi:10.1038/s41434-021-00263-9 (2021).
778   39   Erwood, S. *et al.* Saturation variant interpretation using CRISPR prime editing.
779   *bioRxiv*, 2021.2005.2011.443710, doi:10.1101/2021.05.11.443710 (2021).
780   40   Choi, J. *et al.* A temporally resolved, multiplex molecular recorder based on
781   sequential genome editing. *bioRxiv*, 2021.2011.2005.467388,
782   doi:10.1101/2021.11.05.467388 (2021).
783   41   Chen, W. *et al.* Multiplex genomic recording of enhancer and signal transduction
784   activity in mammalian cells. *bioRxiv*, 2021.2011.2005.467434,
785   doi:10.1101/2021.11.05.467434 (2021).
786   42   Loveless, T. B. *et al.* Molecular recording of sequential cellular events into DNA.
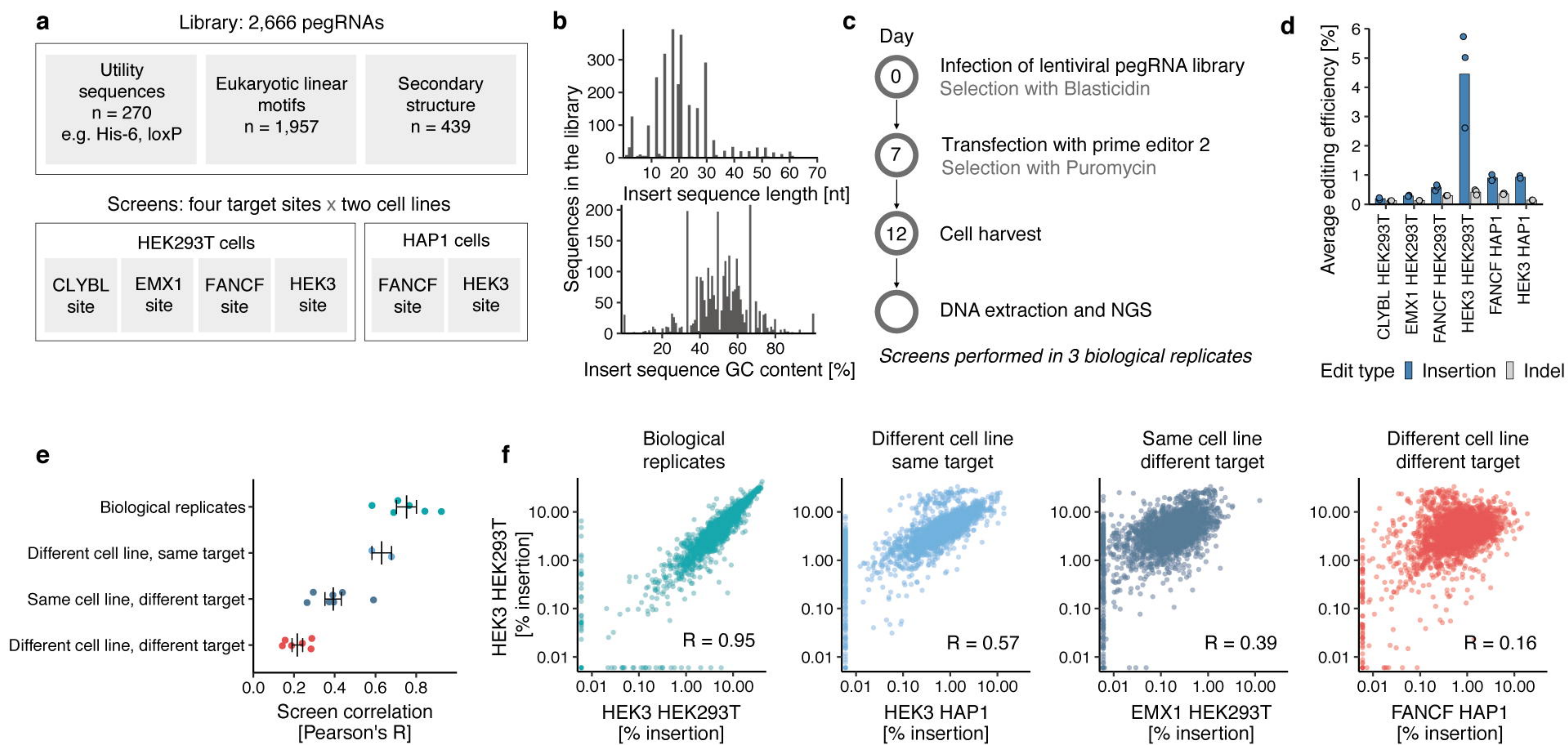787   *bioRxiv*, 2021.2011.2005.467507, doi:10.1101/2021.11.05.467507 (2021).
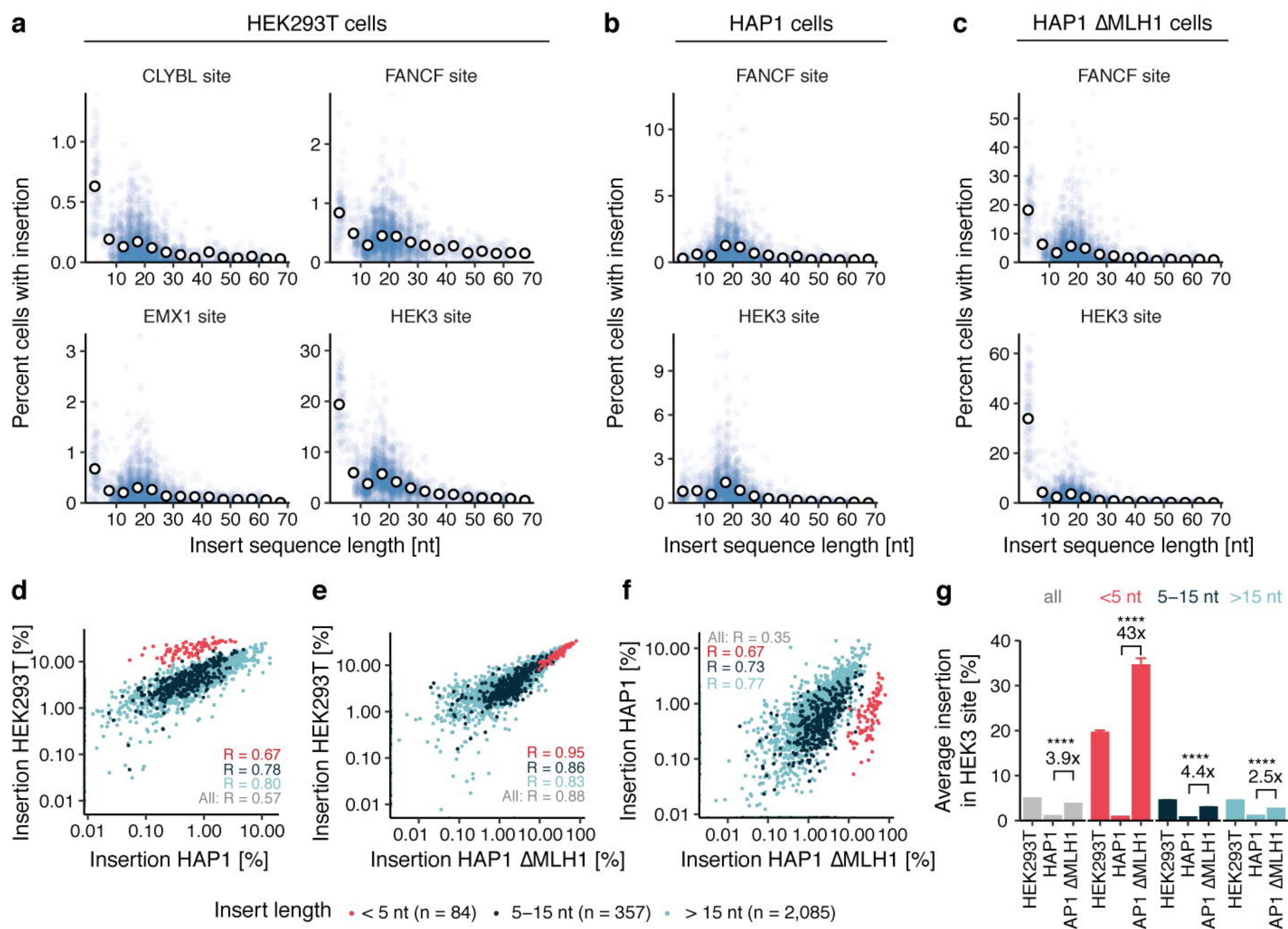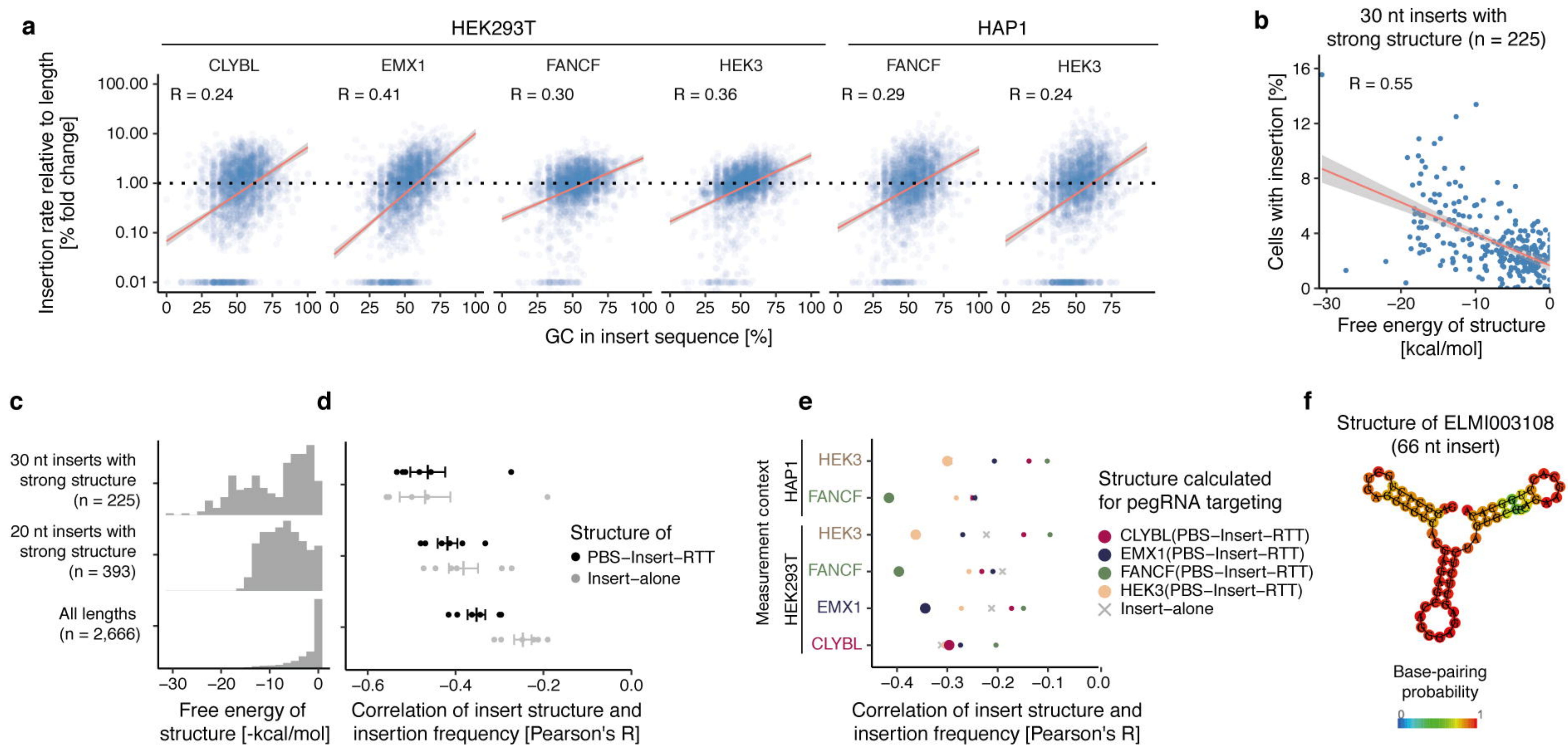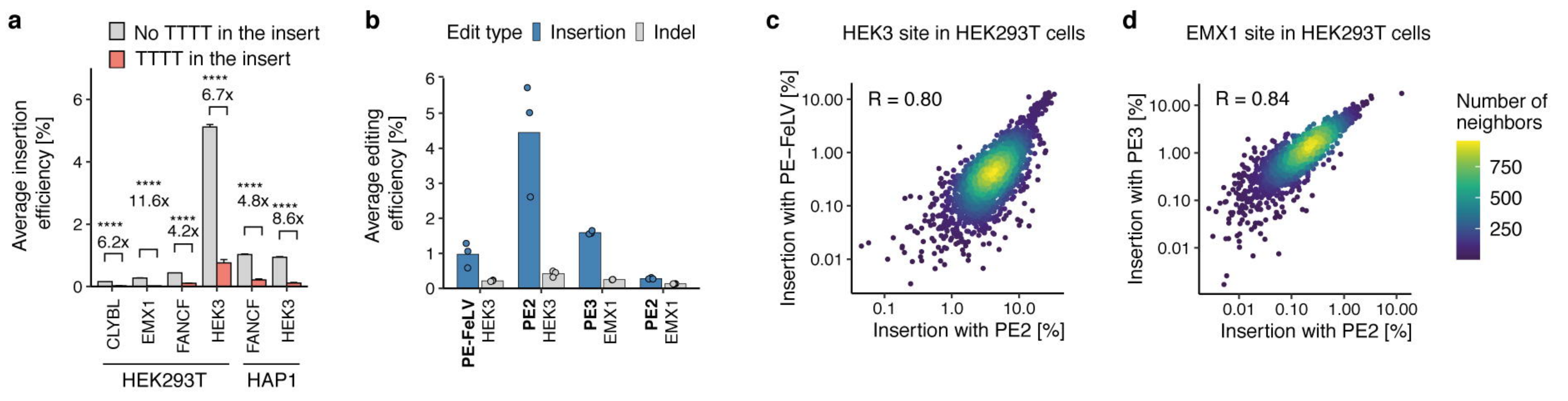788

Figure 1

Figure 2

Figure 3

Figure 4

a

Prediction accuracy [Pearson's R]

Lasso regression
Ridge regression
Random forest
Multi-layer perceptron
XGBoost

b

Model with MMR
Model without MMR

Prediction accuracy [Pearson's R]

*** *** **

CLYBL EMX1 FANCF HEK3 | FANCF HEK3 | FANCF HEK3

HEK293T | HAP1 | HAP1 dMLH1

Tested dataset

c

Predicted [z-score]

Measured [z-score]

Pearson's R = 0.69

d

Length
Secondary structure 3'-extension
C content [%]
Secondary structure insert
Count A
Count T
Melting temperature
GC content [%]
A content [%]
T content [%]

High
Low
Feature value

SHAP value (impact on model output)

e

HEK3 site in HEK293T cells

Measurement | Prediction

His6-tag

CACCACCACCACCACCAC
CATCACCATCACCATCAC
CATCATCATCATCATCAT
CATCATCATCACCACCAC
GTGGTGGTGGTGGTGGTG
ATGATGATGATGATGATG
GTGGTGGTGATGATGATG
GTGATGGTGATGGTGATG

CACCACCACCACCACCAC
CATCACCATCACCATCAC
CATCATCATCACCACCAC
CATCATCATCATCATCAT
GTGGTGGTGGTGGTGGTG
ATGATGATGATGATGATG
GTGGTGGTGATGATGATG
GTGATGGTGATGGTGATG

20 0 | 0 5
Insertion rate [%]